1 *Article*

2 Statistical validation verifies that enantiomorphic
3 states of cell chirality are determinant dictating the
4 left- or right-handed direction of the hindgut rotation
5 in *Drosophila*

6 **Tomoki Ishibashi [1], Mikiko Inaki [2], Kenji Matsuno [2,*]**

7 [1] Graduate School of Agriculture, Kyoto University; ishibashi.tomoki.5m@kyoto-u.ac.jp
8 [2] Department of Biological Sciences, Graduate School of Science, Osaka University
9 * Correspondence: kmatsuno@bio.sci.osaka-u.ac.jp

10 **Abstract:** In the left-right (LR) asymmetric development of invertebrates, chirality of cells (cell
11 chirality) plays crucial roles. Left- or right-handed structure of cells consequently directs the
12 morphogenesis with corresponding LR asymmetry. In *Drosophila*, it has been suggested that cell
13 chirality drives the LR-asymmetric development of various organs including the embryonic hindgut.
14 However, this hypothesis is supported only by apparent concordance between these two events and
15 by computer simulations connecting them [1–5]. Therefore, here, we mathematically evaluated the
16 causal relationship between the cell chirality of the hindgut epithelial cells and the LR-directional
17 rotation of the hindgut, which was previously postulated. Our logistic model obtained from various
18 genetic backgrounds significantly explained the correlation between the enantiomorphic states of
19 cell chirality and the LR directionality of hindgut rotation. This model also significantly explained
20 the correlation between cell chirality stochastically formed in advance in each living embryo and
21 the LR-directionality of the following rotation, suggesting the irrelevance of modes how cell
22 chirality is formed. This analysis also showed that the cell chirality is not only sufficient but also
23 required for the rotation. Considering the chronological order of these events, our study validated
24 that cell chirality causally defines the LR asymmetry of the hindgut rotation.

25 **Keywords:** Cell chirality; Left-right asymmetry; Gut; Development; *Drosophila*

26

27 1. Introduction

28   Left-right (LR) asymmetry is often integrated into the basic body plan in bilaterians. For example,
29 internal organs of bilaterians are often LR asymmetric in their morphology and functions. The
30 mechanisms of LR asymmetric development have been well studied in vertebrates [6–10]. For example,
31 in mice, motile cilia locating in the node rotates clockwise and induces a leftward flow of extra-
32 embryonic fluid, which first breaks the LR symmetry [11]. This phenomenon is called as "nodal flow"
33 that subsequently induces the left-side-specific expression of genes, such as *Nodal* and *Lefty*, required
34 for the LR asymmetric development of organs [11–13]. The mechanisms of the LR symmetry breaking
35 are evolutionarily diverged even among vertebrates. For example, in reptile and chick, the nodal
36 flow-independent mechanisms of the LR-symmetry breaking were reported [14,15]. In invertebrates,
37 the chirality of cells (cell chirality) contributes to their LR-asymmetric development [16–18]. An object,
38 such as a cell, is chiral if it cannot be superimposed onto its mirror image. In snails and nematodes,
39 the cell chirality of blastomeres at the initial stage of cleavage determines the subsequent LR-
40 asymmetric arrangement of them, which consequently directs the LR asymmetry of their whole
41 bodies [19,20].
42   *Drosophila* has various organs showing stereotypic LR asymmetry, which include, for example,
43 the embryonic gut, male genitalia, and brain [21–29]. The embryonic hindgut is the first organ that shows
44 LR asymmetry during the development of this species [21]. The hindgut is formed in a bilaterally

symmetric structure whose anterior part curves toward the ventral side of the embryo and subsequently rotates counterclockwise 90°, which makes it bent rightward [21]. It was shown that the active force for driving the hindgut rotation is generated by the hindgut epithelial tube [2,30]. Before the rotation, apical cell-boundaries of the hindgut epithelial cells slant leftward with respect to the anterior-posterior axis of this organ [1–3,31]. Considering the apical-basal polarity of the hindgut epithelial cells, the three-dimensional structure of them has cell chirality [1]. During the rotation, the cell chirality eventually dissolved so that the cell shape becomes bilaterally symmetric after the rotation of the hindgut [1]. Cooperative studies between computer simulations involving vertex models and image analysis of the hindgut epithelium suggested that the dissolution of the cell chirality induces "cell sliding," which leads to the LR-asymmetric rotation of the hindgut epithelial tube [1,2]. In cell sliding, the epithelial cells LR-asymmetrically changes their relative position without cell-junctional remodeling, which is coupled with the tube rotation to the corresponding LR directions [2]. Contributions of cell chirality to the LR-asymmetric development were reported in other LR asymmetric organs in *Drosophila*, suggesting that cell chirality has general roles in the LR-asymmetric development of this species [4,25,32,33]. Not only in snails, nematodes, and *Drosophila* but also in Chordata, such as chicken and Larvaceans, the cell chirality was observed and suggested to be involved in the LR asymmetric development of these species [34,35]. In addition to the cell chirality observed *in vivo* during development, various cultured cells from *Dictyostelium* to humans demonstrate intrinsic chirality in their structure and movement [36–40]. Thus, cell chirality is a widely observed property shared among eukaryotic cells.

Using *Drosophila* as a model system, genetic mechanisms underlying the formation of cell chirality has been studied [1,31,33]. *MyosinID* (*MyoID*), a Myosin I family gene and also called *Myosin31DF*, has an activity to induce dextral cell chirality, so that the loss-of-function mutations of *MyoID* resulted in the sinistral cell chirality and the LR-inversion of various organs demonstrating dextral LR asymmetry in wild-type, including the embryonic hindgut [1–5,25,31,33]. *MyosinIC* (*MyoIC*), also called *Myosin61F* and belonging to Myosin I family, bears an activity to induce sinistral cell chirality, which leads to the LR inversion of various organs with handedness upon its overexpression [5,22,30,41]. Besides these Myosin I family genes, we previously found that the loss-of-function mutations of *extra macrochaetae* (*emc*) gene, the *Drosophila* ortholog of *Id*, show the randomization of the hindgut handedness [31]. Id family genes encode class V helix-loop-helix (HLH) proteins that inhibit E-box proteins, a class of basic HLH transcriptional factors such as Daughterless (Da) in *Drosophila*, by forming heterodimer, which regulates the balance between cell differentiation and cell proliferation [42]. We found the *MyoID* functions downstream of or parallel to *emc* in the cell chirality formation [31]. However, although genetic mechanisms of cell chirality formation began to be understood, the causal relationship between the cell chirality and hindgut rotation was predicted only on apparent concordance between the enantiomorphic states of cell chirality and the directions of the hindgut rotation in various mutants and on the results of computer simulation recapitulating the rotation of the model gut tube driven by the dissolution of cell chirality [1,2]. Therefore, the validity of such a cause and effect relationship was still needed.

Here, we mathematically evaluated the causal relationship between the cell chirality and hindgut rotation. We developed a new live-imaging procedure to analyze the cell chirality and subsequent rotation of the hindgut, which provides an opportunity to test the cause and effect relationship between them. Our study validated that the enantiomorphic states of cell chirality causally defines the LR asymmetry of the hindgut rotation.

2. Materials and Methods

2.1 Fly lines

Canton-S was used as wild-type. The following mutants were used: *emc^AP6*, an amorphic allele (Bloomington #36544) [43]; *da^10*, an amorphic allele (Bloomington #5531) [44]; and *MyoID^K2*, an amorphic allele [45]. The following UAS lines were used: *UAS-emc::GFP* [46]; *UAS-da* (Bloomington #51669) [47];

95 *UAS-MyoIC* [22]; *UAS-MyoID::mRFP* [3]; and *UAS-myr::GFP* [48]. The following *Gal4*-driver lines were
96 used: *NP2432* (Kyoto DGRC #104201) [49] for the analysis of fixed cell chirality index, and *byn-Gal4* [22]
97 for the analysis of live cell chirality index. Mutations on the second chromosome and third
98 chromosome were balanced with *CyO, P{en1}wg^{en11}* and *TM3, P{GAL4-twi.G}2.3, P{UAS-*
99 *2xEGFP}AH2.3, Sb^1 Ser^1*, respectively. All genetic crosses were carried out at 25°C on a standard
100 *Drosophila* culture medium.

101   *2.2 Live Imaging and laterality score*

102   To visualize the cell membrane of the hindgut epithelium, the expression of *UAS-myr::GFP* was
103 driven by *byn-Gal4* using GAL4/UAS system [50]. *Drosophila* embryos were dechorionated and placed
104 on grape juice agar plates. Embryos of the appropriate genotypes were selected at early stage 12
105 under a fluorescence microscope and mounted dorsal side up on double sticky tape on slide glasses.
106 These embryos were overlaid by oxygen-permeable Halocarbon oil 27 (Sigma, USA) and a coverslip
107 with spacers of 0.17-0.25 mm-thick coverslips. The live images of apical cell-boundaries in hindgut
108 epithelium were obtained with a scanning laser confocal microscope, LSM 880 (Carl Zeiss, Germany)
109 before the onset of the hindgut rotation. After the imaging, the embryos were continuously cultured
110 at 25°C for 3 hours and the rotational directions of the hindgut were evaluated. As laterality score,
111 the hindgut rotating to the counter-clockwise and clockwise directions was scored 1 and 0,
112 respectively. When the hindgut did not rotate, the laterality score was marked as 0.5.

113   *2.3 Analysis of cell chirality index*

114   Cell chirality was analyzed as previously described [31]. Briefly, we obtained the images of apical
115 cell boundaries, which were detected by Myr::GFP signal, in the dorsal part of the embryonic hindgut
116 just before its rotation (at stage 12) using a confocal microscope (LSM880, Carl Zeiss, Germany). Based
117 on these images, the angles (θ) between the anterior-posterior axis of the hindgut tube and each cell
118 boundary were determined by ImageJ Fiji v.2.0.0 [51]. To quantify the LR asymmetric slanting of the
119 apical cell boundaries in the hindgut epithelial cells, a cell chirality index was calculated as $(N_R - N_L)/(N_R + N_L)$, where N_R was the number of boundaries with $0° < \theta < 90°$ and $-180° < -90°$, and
120 N_L was the number of boundaries with $-90° < \theta < 0°$ and $90° < \theta < 180°$, for each embryo. The
121 N_L was the number of boundaries with $-90° < \theta < 0°$ and $90° < \theta < 180°$, for each embryo. The
122 chirality index was measured in a double-blind manner, in which the person analyzing the cell
123 boundaries did not know the genotypes of the embryos and the prospective rotational direction of
124 the hindgut.

125   *2.4 Statistical analysis*

126   To test the correlation between the mean cell chirality and the mean of the laterality score in
127 fixed embryos or between the live chirality index and the laterality score in each living embryo,
128 logistic models were used [52]. As a null hypothesis, naive models were used [52]. For the fixed embryos,
129 the mean of laterality score was treated as a response variable, and the mean of the cell chirality index
130 was treated as an explanatory variable. For the live embryos, the laterality score of each individual
131 embryo (0, 0.5, or 1) was treated as a response variable, and the live cell chirality index of each was
132 treated as an explanatory variable. All statistical analyses were performed using R software v.3.6.3 [53].
133 Graphs were prepared using Matplotlib v.3.0.3 in Python v.3.6.4 [54,55].

134 **3. Results**

135   *3.1 A logistic model significantly explained the correlation between the enantiomorphic states of cell*
136 *chirality and the LR directionality of hindgut rotation*

137   The *Drosophila* hindgut is first formed as a bilaterally symmetric invagination whose anterior
138 part curves ventrally at early stage 12 (Figure 1A most left panel) [22]. Then, it gradually rotates
139 counterclockwise 90° as a view from the posterior (Figure 1A, middle two panels). Consequently,
140 this rotation makes the hindgut curved towards the right at the end of stage 13 (Figure 1A, most right

141 panel). The hindgut epithelium has a typical apical-basal polarity, and the inner surface of the
142 hindgut corresponds to the apical surface. Before the rotation of the hindgut, cell chirality of the
143 hindgut epithelial cells is detected in the shape of their apical surface, as the frequency of cell
144 boundaries that slant left or right with respect to the anterior-posterior axis of the hindgut tube shows
145 deviations according to the genetic conditions [31]. For example, cell-boundaries slanting to the left
146 appeared more often than that of the right in wild-type (Figure 1B, left). However, such LR bias found
147 in the angle of cell boundaries is dissolved after the completion of the hindgut rotation (Figure 1B,
148 right). To quantitatively analyze the cell chirality, "chirality index" was formulated previously [31].
149 The apical cell boundaries were visualized, and the origin of two-dimensional coordinate
150 corresponding the anterior-posterior and left-right axes are placed on a vertex (Figure 1C most left).
151 The cell boundaries exist in the first and third quadrants (shown in orange) and the second and fourth
152 quadrants (shown in turquoise) are defied as Right (orange lines) and Left (turquoise lines),
153 respectively (Figure 1C left and middle). Then, the total numbers of Right and Left were represented
154 by N-Right (N_R) and N-Left (N_L), respectively (Figure 1C, right). The average values of the cell
155 chirality index obtained from embryos (numbers are indicated in Figure 2B as N_x) with each
156 genotype were referred to as "mean cell chirality index."

157 We previously showed that the mean cell chirality index strongly correlated with the ratio of the
158 normal hindgut laterality in embryos with various genotypes [31]. To investigate a causal association
159 between the enantiomorphic states of cell chirality and the LR directions of the hindgut rotation, we
160 here analyzed the mathematical characteristics of the correlation between the mean cell chirality
161 index and the rotational direction of the hindgut. We scored the rotational direction of the hindgut
162 in each embryo as a "laterality score", in which the hindgut of normal LR asymmetry, non-laterality
163 (bilateral symmetry), and inverse LR asymmetry was scored 1, 0.5, and 0, respectively (Figure 2A).
164 The mean of the laterality score was calculated in embryos with each genotype (Figure 2B). Besides
165 the eight genetic conditions analyzed in the previous study, we examined two additions to study the
166 correlation between the mean cell chirality index and the mean of the laterality score (Figure 2B) [31].
167 As the newly added conditions, double mutant embryos of da^{10} and emc^{AP6} (da^{10}; emc^{AP6}) were analyzed
168 (Figure 2B). Our previous analysis revealed that da mutation suppresses the LR defects of the hindgut
169 in emc mutant because emc mutant induces the LR defects through the hyper-activation of da [31].
170 Additionally, embryos overexpressing UAS-$MyoIC$, which has the sinistral activity of the LR
171 asymmetric development, in the hindgut epithelium were examined (Figure 2B) [5,30,41].

172 We fitted the logistic model (dotted line) with the chirality index as an explanatory valuable and
173 the mean of the laterality score as an objective variable (Figure 2B). The chirality index significantly
174 explained the mean of laterality score (Quasibinomial generalized linear model (GLM), two-tailed t-
175 test, $p < 0.001$) (Figure 2B, Table S1).

176 *3.2 Cell chirality index predicts the LR directions of future hindgut rotation in live embryos*

177 Considering that the cell chirality appears before the initiation of the hindgut rotation, the
178 significant correlation between the mean cell chirality index and the mean of laterality score
179 suggested that cell chirality index of each embryo may determine the LR directionality of the hindgut
180 rotation in an individual. In this case, the chirality index in each live embryo should predict the left
181 or right directionality of the future hindgut rotation afterward. To test this possibility, we developed
182 a new procedure to obtain the cell chirality index in the hindgut of live embryos and then determine
183 the subsequent LR directionality of the hindgut rotation. In this system, the apical cell boundaries of
184 the hindgut epithelium were visualized in live embryos at early stage 12 under a confocal laser
185 microscope, and these embryos were continuously cultured another three hours (Figure 3A). At that
186 point, the rotation of the hindgut was completed under these conditions in wild-type (Figure 3A
187 right). The cell chirality index obtained from this procedure was designated as "live cell chirality
188 index," and the laterality score of each embryo was marked 1, 0.5, and 0 as the hindgut subsequently
189 showed normal LR asymmetry, non-laterality (bilateral symmetry), and inverse LR asymmetry,
190 respectively.

191   To investigate whether the live cell chirality index correlates with the rotational direction of the
192 hindgut, we found that the LR-randomization phenotypes of *emc^AP6* homozygote were appropriate
193 for this purpose. Only in *emc^AP6* mutant among the ten different mutants examined here, the mean
194 cell chirality index was nearly zero with deviation ranging from plus to minus values (Figure 2B). In
195 addition, the hindgut of these embryos shows normal and inverse LR asymmetry as well as non-
196 laterality [31]. Thus, we speculated that each individual embryo has stochastically fluctuated cell
197 chirality, which may induce the hindgut rotation to the direction corresponding to the cell chirality
198 index of each. Based on this assumption, we evaluated the consistency between the chirality indexes
199 obtained from fixed and live embryos, we analyzed the mean of live chirality indexes in wild-type
200 and *emc^AP6* homozygous embryos. The mean live chirality indexes of wild-type and *emc^AP6*
201 homozygous embryos were -0.12 ± 0.04 and -0.02 ± 0.03, respectively, which were very similar
202 to those of fixed embryos as reported before (wild-type, -0.11 ± 0.03; *emc^AP6* homozygote, $0.01 \pm$
203 0.02), although these mean values of live cell chirality indexes were not significantly different in this
204 experiment (Two-tailed t-test, $p = 0.069217$) [31]. We also found that each individual embryo of *emc^AP6*
205 homozygote showed a broad range of live chirality indexes, which were distributed from plus to
206 minus values, as compared with that of wild-type (Figure 3B).

207   Given that the values of the live chirality index agreed well with those of the cell chirality index
208 in the fixed embryos, we next conducted a statistical correlation analysis between the live cell chirality
209 index and the laterality score of each individual *emc^AP6* mutant embryo. We fitted the logistic model
210 (solid line) with the live chirality index as an explanatory variable and the laterality score of each
211 embryo as an objective variable and found that live cell chirality, which was determined prior to the
212 onset of the hindgut rotational direction significantly explained the rotational directions of the
213 hindgut (Quasibinomial GLM, two-tailed t-test, $p < 0.01$; Figure 3C; Table S2). Importantly, the
214 logistic model (dotted line) obtained the fixed embryos with various genetic conditions as described
215 in Figure 2 significantly fitted the data obtained from each living *emc^AP6* mutant embryo
216 (Quasibinomial GLM, likelihood ratio test, $\chi_1^2 = 4.327$, $p < 0.05$), and it explained 72.5% of the total
217 variation in the rotational direction of live *emc^AP6* mutant hindgut (Table S3). These results suggested
218 that the cell chirality index correlates with the rotational direction of the hindgut, disregarding that
219 the enantiomorphic states of cell chirality are determined by genetic conditions or stochastic
220 fluctuations. Although, with just a statistical correlation, we could not conclude whether cell chirality
221 is the cause or effect. Nevertheless, considering the clear chronological sequence of the cell chirality
222 formation and the initiation of the hindgut rotation, we concluded that the enantiomorphic states of
223 cell chirality direct the LR asymmetry of the hindgut rotation.

224 **4. Discussion**

225   In previous studies, it was suggested that the enantiomorphic states of cell chirality in the
226 hindgut epithelium determine the directionality of the hindgut rotation [1,2,31]. Mainly, dextral and
227 sinistral cell chirality on average lead to the counter-clockwise and clockwise rotation of the hindgut,
228 respectively [1,2]. This postulation was firstly supported by the observations that the mean states of
229 cell chirality and the LR directions of the hindgut rotation correlate to each other in various mutants
230 [1,2,31]. For example, in *MyoID* mutants where cell chirality becomes sinistral, their hindgut rotates
231 clockwise, whereas wild-type embryos demonstrate dextral cell chirality and the counter-clockwise
232 rotation of the hindgut[1]. Additionally, the cell chirality vanishes on average in *Drosophila E-cadherin*
233 or *emc* mutants in which the LR-directions of hindgut rotation are randomized or the hindgut remains
234 LR symmetric [1,31]. Secondary, computer simulation employing vertex models suggested that the
235 enantiomorphic states of cell chirality initially introduced into the model defines the LR direction of
236 the model-gut tube rotation and successively drives the tube rotation to the direction determined at
237 the outset [1]. Although these evidences consistently support the postulation, the hypothesis has been
238 grounded on the apparent concordance between the states of cell chirality and the LR directions of
239 the hindgut rotation and on the prediction from computer simulations [1,2]. Thus, the cause and effect
240 relationship between them needed to be verified.

241   To address this issue, here, we mathematically evaluated this hypothetical causal relationship
242   by analyzing the correlation between the enantiomorphic states of cell chirality and the LR direction
243   of the hindgut rotation. The means of the cell chirality index and laterality score in the fixed embryos
244   were obtained for each of ten different genetic conditions, and the correlation between them was
245   analyzed. In our logistic model, the mean cell chirality index representing each genotype as an
246   explanatory variable significantly fitted to the mean of the laterality score (Figure 2B). Therefore, the
247   mechanisms by which the cell chirality defines the LR-directionality of the hindgut rotation may be
248   similar regardless of genetic backgrounds. This result also demonstrates that the LR directionality of
249   the hindgut rotation is statistically explained even only by the enantiomorphic states of cell chirality
250   as the average of embryos with each specific genotype.

251   In the correlation analysis of the fixed embryos, the mean of cell chirality index was 0.01 ± 0.02
252   in *emc^{AP6}* mutant embryos, nevertheless, they showed the hindgut rotating to the directions of either
253   clockwise or counter-clockwise or staying as bilaterally symmetric shape (Figure 2B) [31]. Thus, one
254   can argue that cell chirality may not be essential for directing the hindgut rotation. Our analyses here
255   addressed this question. In this study, we developed a method to determine the live cell chirality and
256   the directions of the hindgut rotation in each living embryo. We found that the live cell chirality
257   indexes representing each individual embryo of *emc^{AP6}* mutant are varied widely among embryos
258   and distributed from plus to minus values, although the mean value of the live cell chirality index of
259   these embryos was nearly zero (Figure 3B). Therefore, this mutant background was found useful to
260   analyze the correlation between the states of cell chirality and the rotational directions of the hindgut
261   in each live embryo. Our logistic model formulated from the data of the live *emc^{AP6}* mutant embryos
262   showed a significant correlation between the live cell chirality index and the laterality score of each
263   individual embryo (Figure 3C). Therefore, in each of these embryos, the live cell chirality index
264   significantly explained the rotational directions of the hindgut or its bilateral structure. Based on
265   these results, we ascertained that the cell chirality is not only sufficient but also required for the
266   hindgut rotation because our model predicts that living embryos with zero cell chirality index tend
267   to have bilaterally symmetric hindgut.

268   Importantly, the logistic model obtained from the fixed embryos with various genetic conditions
269   significantly fitted the data obtained from each living *emc^{AP6}* mutant embryo (Quasibinomial GLM,
270   likelihood ratio test, $\chi^2_1 = 4.327$, $p < 0.05$), and it explained 72.5% of the total variation in the
271   rotational direction of *emc^{AP6}* mutant hindgut (Figure 3C; Table S3). Given that individual embryos
272   all carrying the same *emc^{AP6}* mutant background showed a wide range of live cell chirality index, cell
273   chirality may be formed stochastically in each individual under this condition. Nevertheless, the
274   logistic model formulated from the data of fixed embryos with various genotypes significantly
275   explains the data that presumably reflects the stochastic events in each *emc^{AP6}* individual. Therefore,
276   underlying mechanisms in which cell chirality drives the LR-directional rotation of the hindgut are
277   common between the cell chirality formed by the modes determined genetically and stochastically.

278   In this study, we mathematically confirmed the causal relationship between cell chirality and
279   the hindgut rotation. Our logistic model also implied that the cell chirality is sufficient and necessary
280   for the hindgut rotation. Considering the time course of the events in which cell chirality formation
281   precedes the initiation of the LR-directional rotation of the hindgut *in vivo*, our presented results
282   demonstrate that the cell chirality is the primary cause of the hindgut rotation. Since the cell chirality
283   is involved in the LR-asymmetric development of various organs in *Drosophila*, such cause and effect
284   relationship can be applicable to explain their morphogenesis. Furthermore, our idea could be
285   extended to the LR-asymmetric developments in other various species, which are known to involve
286   the cell chirality.

287

Appendix:

	t_8-value	p-value
Intercept	-4.042	0.003723
Chirality Index	-5.992	0.000326

Table S1. Factors affecting the variation in the laterality score of the embryonic hindgut with various genotypes.

	t_{13}-value	p-value
Intercept	-1.149	0.27109
Live Chirality Index	-3.256	0.00625

Table S2. Factors affecting the variation in the rotational direction of the hindgut in *emc^AP6*.

	Model	R^2
Best fit model	$1 - \dfrac{1}{1 + e^{-4.531 \times (x - 0.00697)}}$	0.8607872
Model fitted for Figure 2	$1 - \dfrac{1}{1 + e^{-0.410 \times (x - 3.42)}}$	0.7246853

Table S3. Logistic regression analyses between the laterality score and live chirality index in *emc^AP6*.

312 **Figure legends**

313   **Figure 1. The wild-type *Drosophila* embryonic hindgut rotates 90° counter-clockwise.** (A)
314   The *Drosophila* embryonic hindgut (orange) visualized by the expression of *UAS-myr-GFP*, encoding
315   a cell-membrane marker, driven by *byn-Gal4*. The hindgut has a bilaterally symmetric structure
316   whose anterior part curves ventrally at early stage 12. In the wild-type, the hindgut subsequently
317   rotates counter-clockwise and this rotation consequently makes this organ curved to the right. At the
318   end of stage 13, the hindgut exhibits a rightward pointing hook shape. L and R indicate left and right,
319   respectively. (B) Before the hindgut rotation (orange), the apical cell-boundaries of the wild-type
320   hindgut epithelial cells tend to slant to the left, which is defined as the dextral cell chirality. After the
321   hindgut rotation (gray), the cell chirality disappears so that these cells become LR symmetric. (C)
322   Schemas summarizing the procedure used to calculate the cell chirality index. The angle between
323   each boundary and the anterior-posterior (AP) axis of the hindgut was determined. LR represents the
324   left-right axis of the hindgut. Each boundary was classified as a right-tilted (orange) or left-tilted
325   boundary (turquoise). The numbers of right-tilted (N_R) and left-tilted (N_L) boundaries were counted,
326   and the cell chirality index was calculated using the formula shown at the right side of the figure.
327   Scale bars in A are 0.25 μm.
328

329   **Figure 2. Cell chirality significantly explains the hindgut LR asymmetry of the fixed embryos**
330   **with various genotype.** (A) Typical examples of the hindgut (shown in orange) demonstrating
331   normal LR asymmetry (Normal), bilateral symmetry (non-laterality), and inversed LR asymmetry
332   (Inverse), which was scored as 1, 0.5, and 0, respectively. (B) Graph showing the correlation between
333   the mean cell chirality and the mean value of the laterality score. Some of the data were adopted from
334   our previous paper [31]. The genotypes are shown in the right panel. N_x and N_y indicate the
335   numbers of embryos used for the analyses of the mean chirality index and the mean of laterality score,
336   respectively. The mean values (circles) and standard errors (colored lines) are shown. Dotted line
337   indicates the logistic model that most fits for the data. The coefficient of determination is shown as
338   R^2. The *p*-value of two-tailed t-test was less than 0.001.
339

340   **Figure 3. Live cell chirality predicts the rotational direction of the hindgut.** (A) Typical images
341   of the hindgut in live embryos. The live images of cell-boundaries visualized by *UAS-myr::GFP* driven
342   by *byn-Gal4* in the hindgut epithelium is shown. At early stage 12, the live cell chirality index of the
343   living hindgut epithelial cells was calculated based on a high magnification image surrounded by the
344   orange square (left panel). After 3 hours of incubation, the laterality score was evaluated as normal
345   LR asymmetry, bilateral symmetry, and inversed LR asymmetry were 1, 0.5, and 0, respectively. (B)
346   Box plot of the live chirality index of the hindgut in the wild-type and *emc^{AP6}* mutant embryos. *N*
347   indicates the number of total embryos analyzed. The *p*-value of two-tailed t-test is shown. (C) Graph
348   showing the correlation between the live cell chirality and the laterality score of the hindgut in *emc*
349   mutant. Solid line indicates the best fitted logistic model (Table S2). Dotted line indicates the logistic
350   model obtained from fixed embryos in Figure 2. The coefficient of determination of each model is
351   shown as R^2. *N* indicates the number of total embryos analyzed.
352

References

1. Taniguchi, K. *et al.* Chirality in planar cell shape contributes to left-right asymmetric epithelial morphogenesis. *Science* **333**, 339–341 (2011).
2. Inaki, M. *et al.* Chiral cell sliding drives left-right asymmetric organ twisting. *eLife* **7**, e32506 (2018).
3. Hatori, R. *et al.* Left-right asymmetry is formed in individual cells by intrinsic cell chirality. *Mechanisms of Development* **133**, 146–162 (2014).
4. Sato, K. *et al.* Left-right asymmetric cell intercalation drives directional collective cell movement in epithelial morphogenesis. *Nature Communications* **6**, (2015).
5. Lebreton, G. *et al.* Molecular to organismal chirality is induced by the conserved myosin 1D. *Science* **362**, 949–952 (2018).
6. Blum, M. & Ott, T. Animal left–right asymmetry. *Current Biology* **28** R301–R304 (2018).
7. Hirokawa, N., Tanaka, Y., Okada, Y. & Takeda, S. Nodal Flow and the Generation of Left-Right Asymmetry. *Cell* **125** 33–45 (2006).
8. Nakamura, T. & Hamada, H. Left-right patterning: conserved and divergent mechanisms. *Development* **139**, 3257–3262 (2012).
9. Levin, M. Left-right asymmetry in embryonic development: A comprehensive review. *Mehanisms of Development* **122** 3–25 (2005).
10. Yoshiba, S. & Hamada, H. Roles of cilia, fluid flow, and Ca^{2+} signaling in breaking of left-right symmetry. *Trends in Genetics* **30** 10–17 (2014).
11. Nonaka, S. *et al.* Randomization of left-right asymmetry due to loss of nodal cilia generating leftward flow of extraembryonic fluid in mice lacking KIF3B motor protein. *Cell* **95**, 829–837 (1998).
12. Nonaka, S., Shiratori, H., Saijoh, Y. & Hamada, H. Determination of left-right patterning of the mouse embryo by artificial nodal flow. *Nature* **418**, 96–99 (2002).
13. Takeda, S. *et al.* Left-right asymmetry and kinesin superfamily protein KIF3a: New insights in determination of laterality and mesoderm induction by *kif3A(-/-)* mice analysis. *Journal of Cell Biology* **145**, 825–836 (1999).
14. Kajikawa, E. *et al.* Nodal paralogues underlie distinct mechanisms for visceral left–right asymmetry in reptiles and mammals. *Nature Ecology and Evolution* **4**, 261–269 (2020).
15. Tabin, C. Do we know anything about how left-right asymmetry is first established in the vertebrate embryo? *Journal of Molecular Histology* **36** 317–323 (2005).
16. Inaki, M., Liu, J. & Matsuno, K. Cell chirality: Its origin and roles in left-right asymmetric development. *Philosophical Transactions of the Royal Society B* **371** (2016).
17. Inaki, M., Sasamura, T. & Matsuno, K. Cell chirality drives left-right asymmetric morphogenesis. *Frontiers in Cell and Developmental Biology* **6**, (2018).
18. Utsunomiya, S. *et al.* Cells with Broken Left–Right Symmetry: Roles of Intrinsic Cell Chirality in Left–Right Asymmetric Epithelial Morphogenesis. *Symmetry* **11**, (2019).
19. Kuroda, R., Endo, B., Abe, M. & Shimizu, M. Chiral blastomere arrangement dictates zygotic left-right asymmetry pathway in snails. *Nature* **462**, 790–794 (2009).
20. Naganathan, S. R. am, Fürthauer, S., Nishikawa, M., Jülicher, F. & Grill, S. W. Active torque generation by the actomyosin cell cortex drives left-right symmetry breaking. *eLife* **3**, e04165 (2014).
21. Hayashi, T. & Murakami, R. Left-right asymmetry in *Drosophila* melanogaster gut development. *Development Growth and Differentiation* **43**, 239–246 (2001).
22. Hozumi, S. *et al.* An unconventional myosin in *Drosophila* reverses the default handedness in visceral organs. *Nature* **440**, 798–802 (2006).
23. Ligoxygakis, P., Strigini, M. & Averof, M. Specification of left-right asymmetry in the embryonic gut of *Drosophila*. *Development* **128**, 1171–4 (2001).
24. Pascual, A., Huang, K. L., Neveu, J. & Préat, T. Brain asymmetry and long-term memory: Fruitflies that have structurally similar brain hemispheres forget within a matter of hours. *Nature* **427**, 605–606 (2004).
25. Spéder, P., Ádám, G. & Noselli, S. Type ID unconventional myosin controls left-right asymmetry in *Drosophila*. *Nature* **440**, 803–807 (2006).
26. Maeda, R. *et al.* Roles of *single-minded* in the left-right asymmetric development of the *Drosophila* embryonic gut. *Mechanisms of Development* **124**, 204–217 (2007).

27. Nakamura, M. *et al.* Reduced cell number in the hindgut epithelium disrupts hindgut left-right asymmetry in a mutant of *pebble*, encoding a RhoGEF, in *Drosophila* embryos. *Mechanisms of Development* **130**, 169–180 (2013).

28. Taniguchi, K. *et al.* D-JNK signaling in visceral muscle cells controls the laterality of the *Drosophila* gut. *Developmental Biology* **311**, 251–263 (2007).

29. Kuroda, J. *et al.* Canonical Wnt signaling in the visceral muscle is required for left-right asymmetric development of the *Drosophila* midgut. *Mechanisms of Development* **128**, 625–639 (2012).

30. Hozumi, S. *et al.* Head region of unconventional myosin I family members is responsible for the organ-specificity of their roles in left-right polarity in *Drosophila*. *Developmental Dynamics* **237**, 3528–3537 (2008).

31. Ishibashi, T. *et al.* E and ID proteins regulate cell chirality and left–right asymmetric development in *Drosophila*. *Genes to Cells* **24**, 214–230 (2019).

32. Coutelis, J. B. *et al. Drosophila* Left/Right Asymmetry Establishment Is Controlled by the Hox Gene *Abdominal-B*. *Developmental Cell* **24**, 89–97 (2013).

33. González-Morales, N. *et al.* The Atypical Cadherin Dachsous Controls Left-Right Asymmetry in *Drosophila*. *Developmental Cell* **33**, 675–689 (2015).

34. Ray, P. *et al.* Intrinsic cellular chirality regulates left–right symmetry breaking during cardiac looping. *Proceedings of the National Academy of Sciences of the United States of America* **115**, E11568–E11577 (2018).

35. Onuma, T. A. *et al.* A chordate species lacking *Nodal* utilizes calcium oscillation and *Bmp* for left–right patterning. *Proceedings of the National Academy of Sciences of the United States of America* **117**, 4188–4198 (2020).

36. Chen, T. H. *et al.* Left-right symmetry breaking in tissue morphogenesis via cytoskeletal mechanics. *Circulation Research* **110**, 551–559 (2012).

37. Tamada, A., Kawase, S., Murakami, F. & Kamiguchi, H. Autonomous right-screw rotation of growth cone filopodia drives neurite turning. *Journal of Cell Biology* **188**, 429–441 (2010).

38. Tee, Y. H. *et al.* Cellular chirality arising from the self-organization of the actin cytoskeleton. *Nature Cell Biology* **17**, 445–457 (2015).

39. Wan, L. Q. *et al.* Micropatterned mammalian cells exhibit phenotype-specific left-right asymmetry. *Proceedings of the National Academy of Sciences of the United States of America* **108**, 12295–12300 (2011).

40. Xu, J. *et al.* Polarity reveals intrinsic cell chirality. *Proceedings of the National Academy of Sciences of the United States of America* **104**, 9296–9300 (2007).

41. Okumura, T. *et al.* Class I myosins have overlapping and specialized functions in left-right asymmetric development in *Drosophila*. *Genetics* **199**, 1183–1199 (2015).

42. Wang, L. H. & Baker, N. E. E Proteins and ID Proteins: Helix-Loop-Helix Partners in Development and Disease. *Developmental Cell* **35** 269–280 (2015).

43. Ellis, H. M. Embryonic expression and function of the *Drosophila* helix-loop-helix gene, *extramacrochaetae*. *Mechanisms of Development* **47**, 65–72 (1994).

44. Wülbeck, C., Fromental-Ramain, C. & Campos-Ortega, J. A. The HLH domain of a zebrafish hE12 homologue can partially substitute for functions of the HLH domain of *Drosophila* DAUGHTERLESS. *Mechanisms of Development* **46**, 73–85 (1994).

45. Petzoldt, A. G. *et al.* DE-Cadherin regulates unconventional Myosin ID and Myosin IC in *Drosophila* left-right asymmetry establishment. *Development* **139**, 1874–1884 (2012).

46. Popova, M. K., He, W., Korenjak, M., Dyson, N. J. & Moon, N.-S. Rb deficiency during *Drosophila* eye development deregulates EMC, causing defects in the development of photoreceptors and cone cells. *Journal of Cell Science* **124**, 4203–4212 (2011).

47. Giebel, B., Stüttem, I., Hinz, U. & Campos-Ortega, J. A. Lethal of Scute requires overexpression of Daughterless to elicit ectopic neuronal development during embryogenesis in *Drosophila*. *Mechanisms of Development* **63**, 75–87 (1997).

48. Pfeiffer, B. D., Truman, J. W. & Rubin, G. M. Using translational enhancers to increase transgene expression in *Drosophila*. *Proceedings of the National Academy of Sciences of the United States of America* **109**, 6626–6631 (2012).

49. Hayashi, S. *et al.* GETDB, a database compiling expression patterns and molecular locations of a collection of gal4 enhancer traps. *Genesis* **34**, 58–61 (2002).

50. Brand, A. H. & Perrimon, N. Targeted gene expression as a means of altering cell fates and generating dominant phenotypes. *Development* **118**, 401–415 (1993).

458   51.   Schindelin, J. *et al.* Fiji: An open-source platform for biological-image analysis. *Nature Methods* **9** 676–682
459   (2012).
460   52.   Campbell, M. J. & Dobson, A. J. An Introduction to Generalized Linear Models. *Biometrics* **47**, 347 (1991).
461   53.   R Core Team. R: A Language and Environment for Statistical Computing. *Vienna, Austria* (2020).
462   54.   Rossum, G. V. & Drake, F. L. Python Tutorial, Technical Report CS-R9526. in *Centrum voor wiskunde en*
463   *informatica (cwi)* (1995). doi:10.1016/j.abb.2004.09.015.
464   55.   Hunter, J. D. Matplotlib: A 2D graphics environment. *Computing in Science and Engineering* **9**, 99–104 (2007).
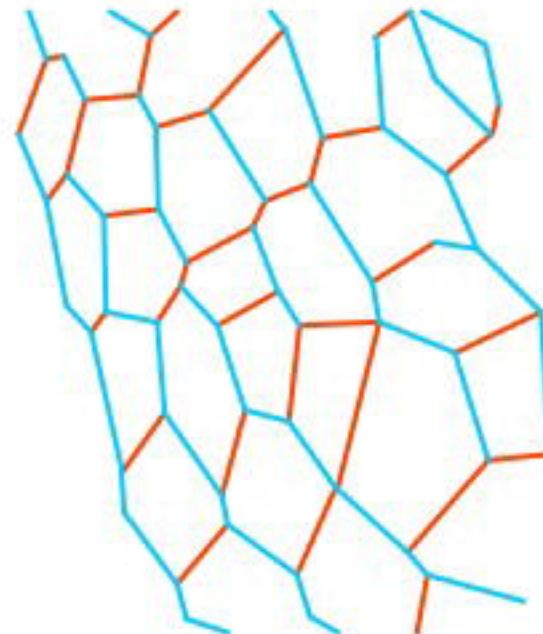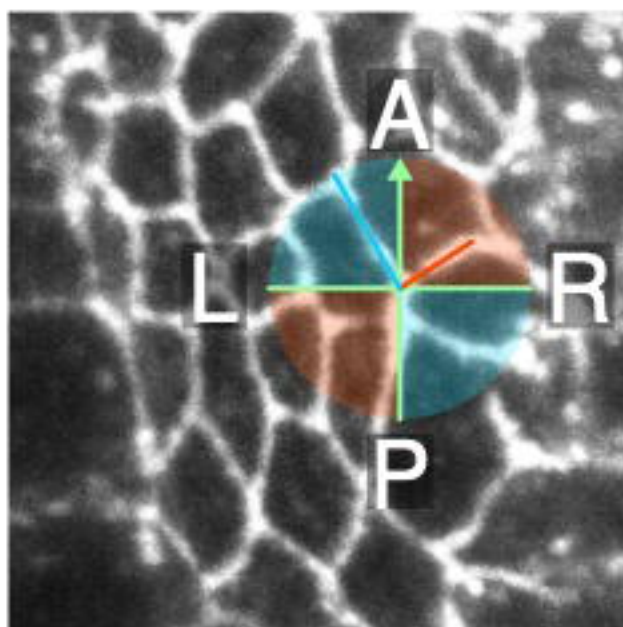
(A) Hindgut

early st.12   L ⟷ R   st.13
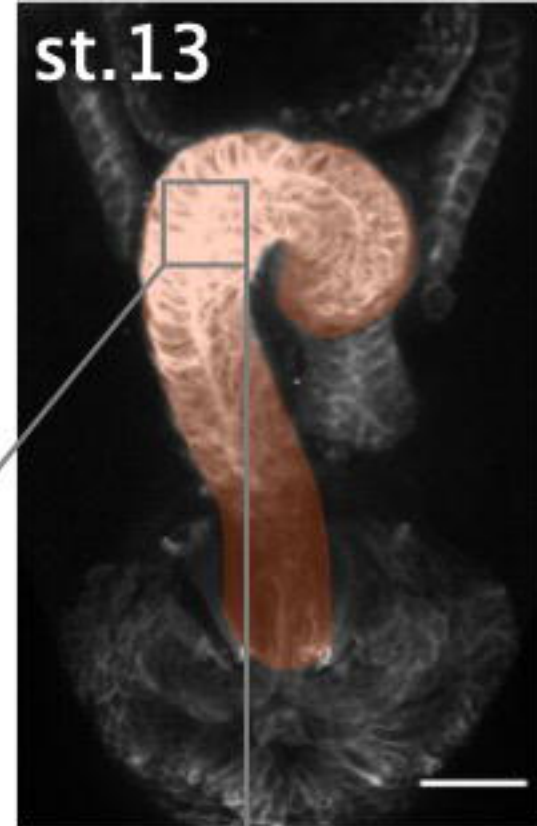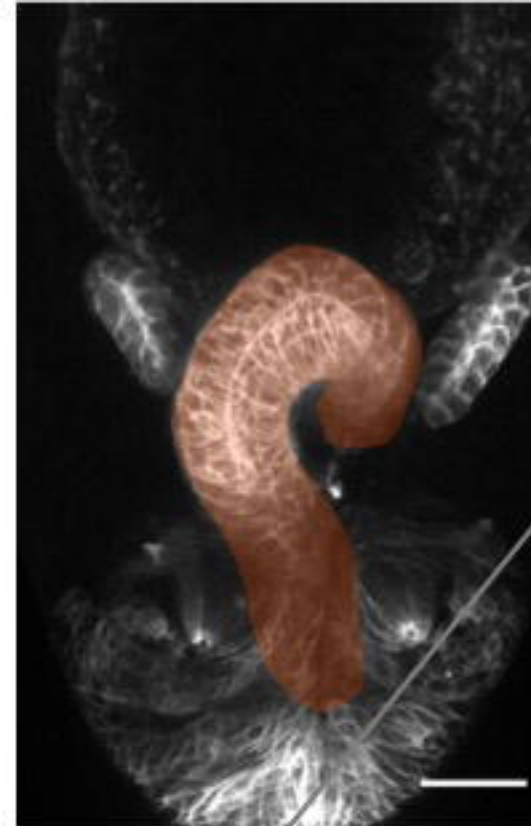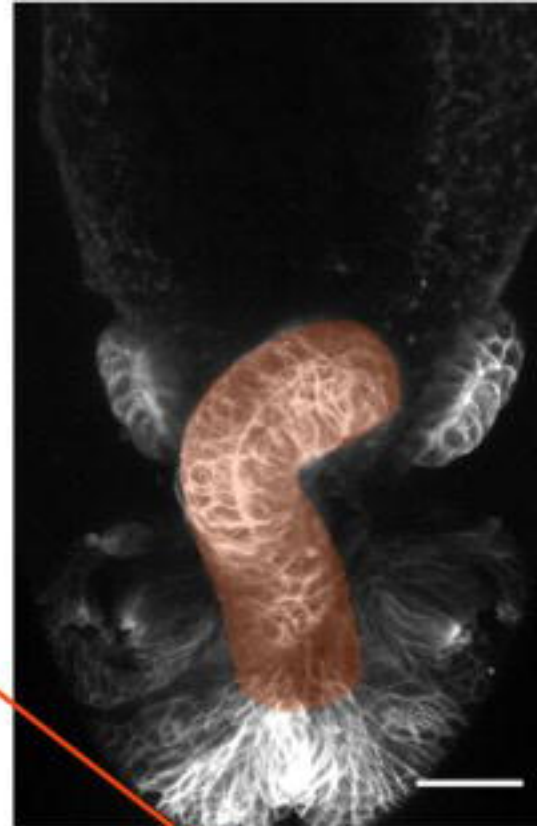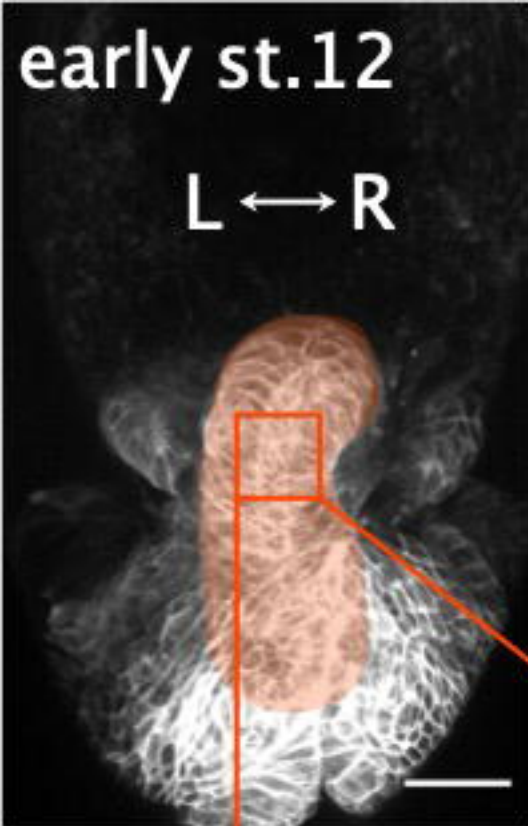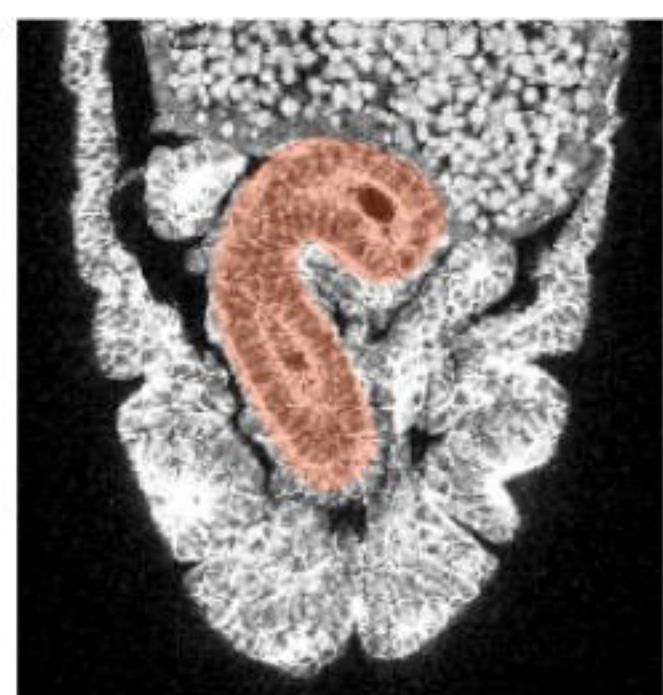
(B) Apical surface of the cells

(C)
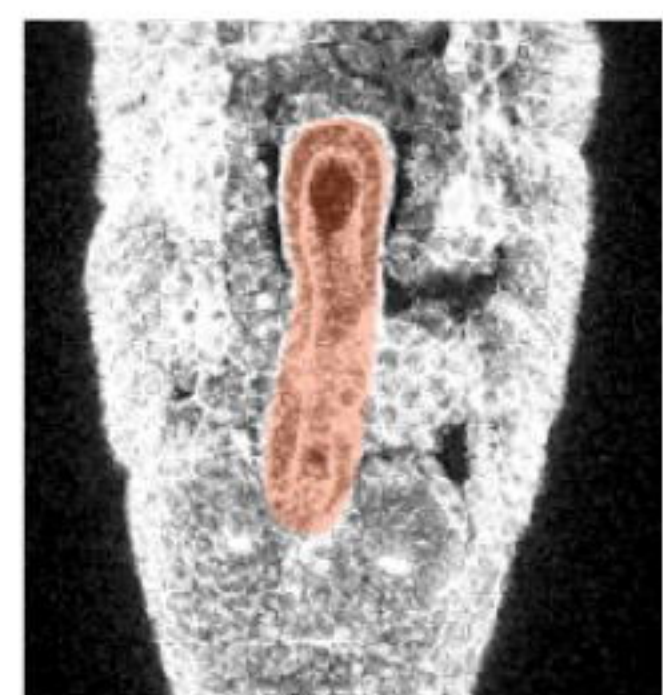
A
L   R
P
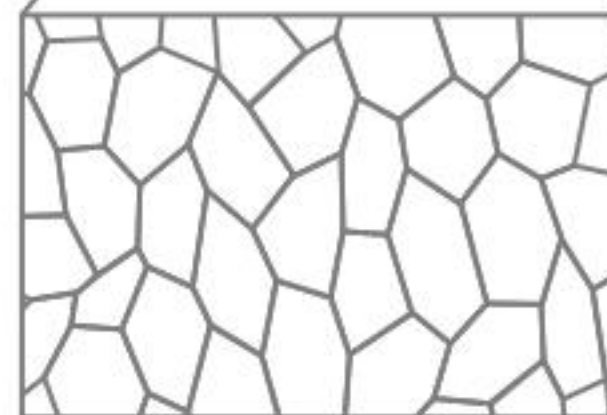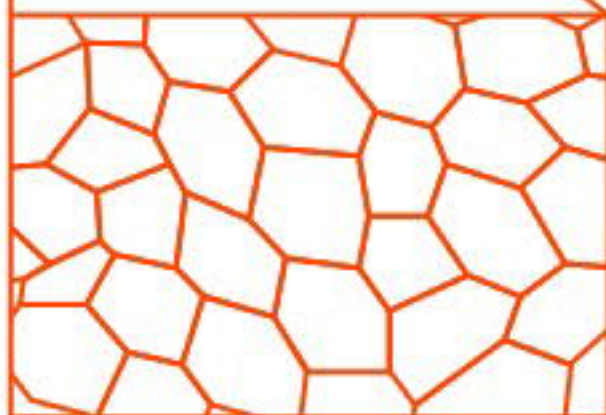
Chirality index

$$\frac{N_R - N_L}{N_R + N_L}$$

(A)

Normal
Score = 1

Non-laterality
Score = 0.5
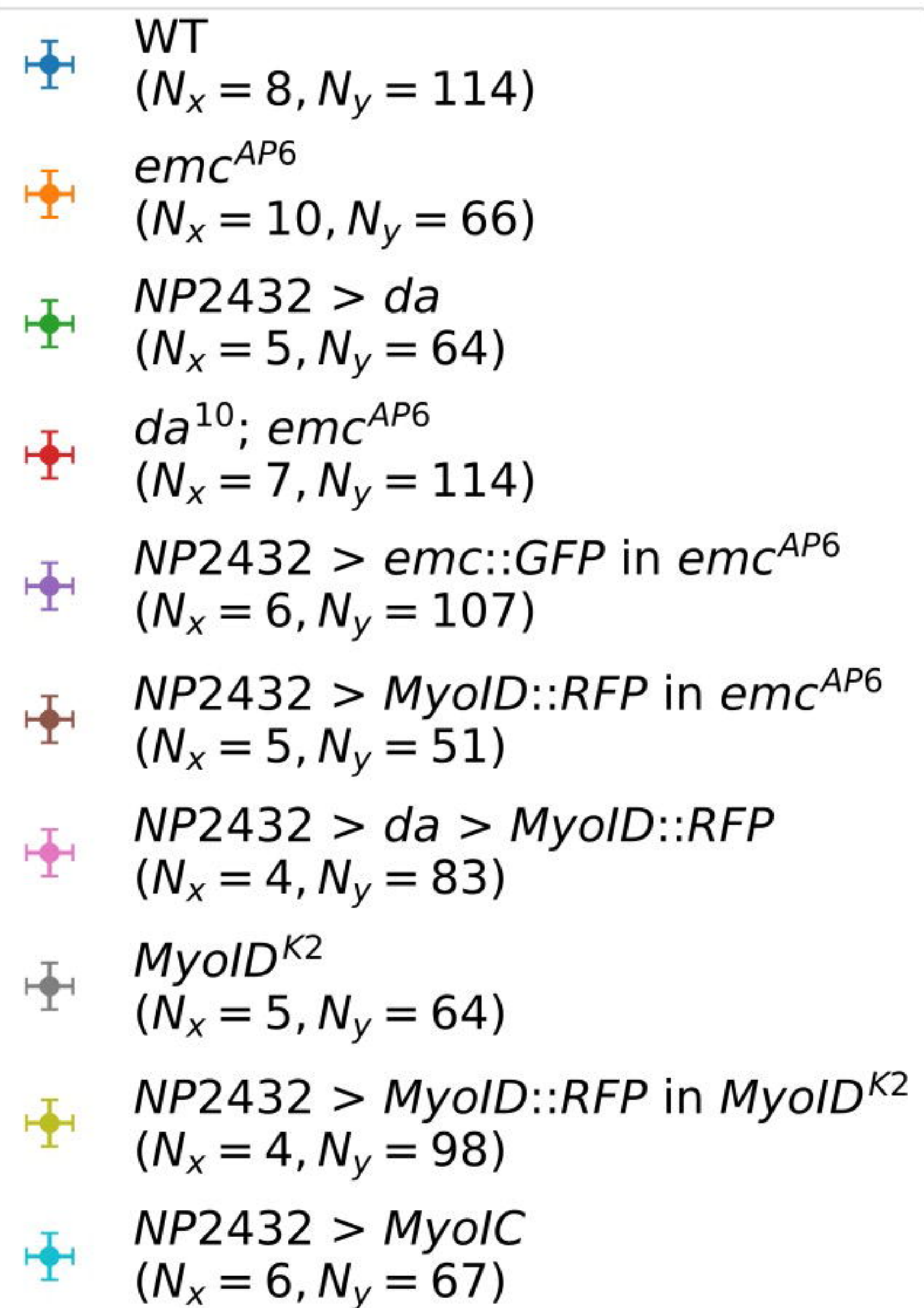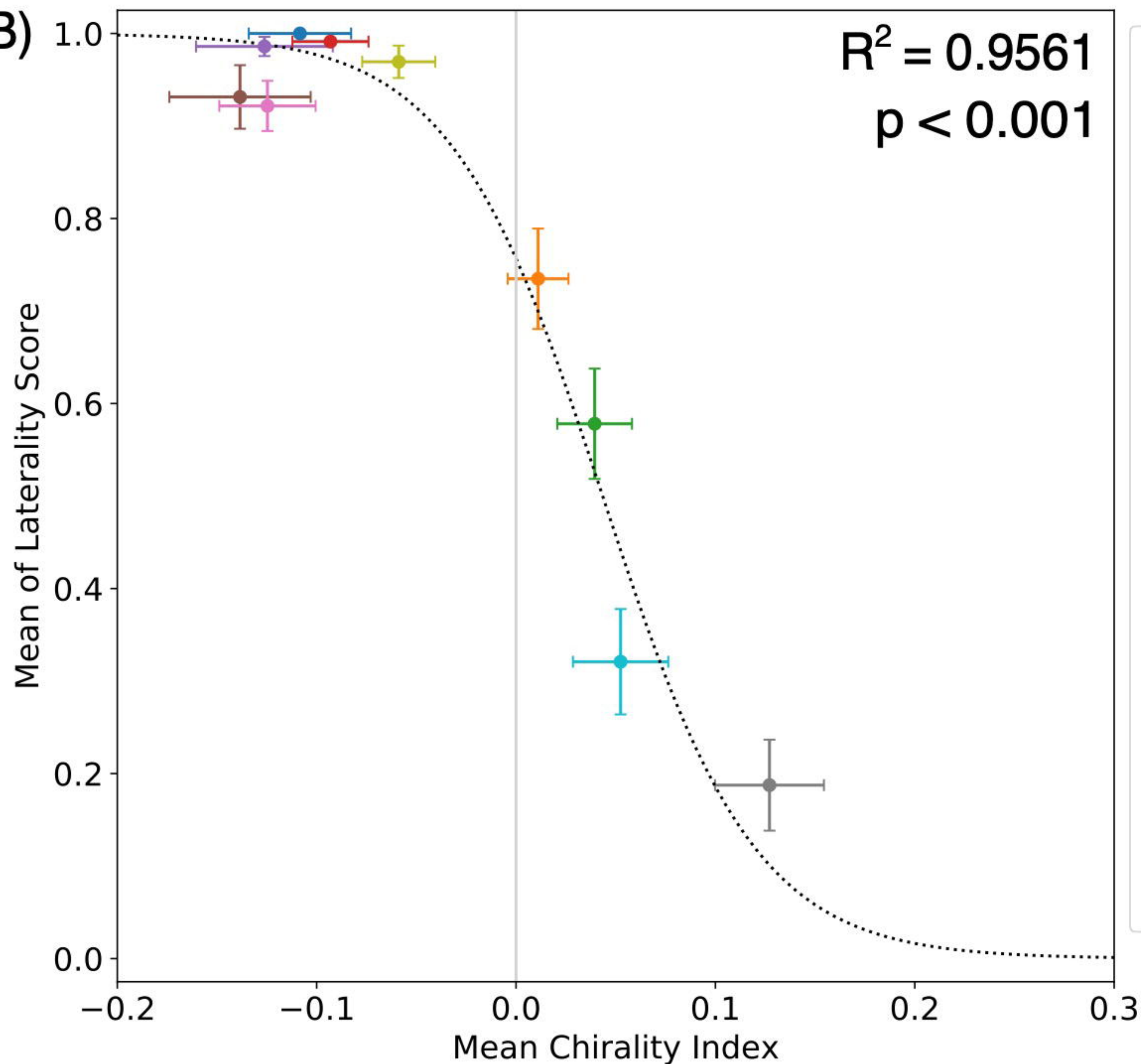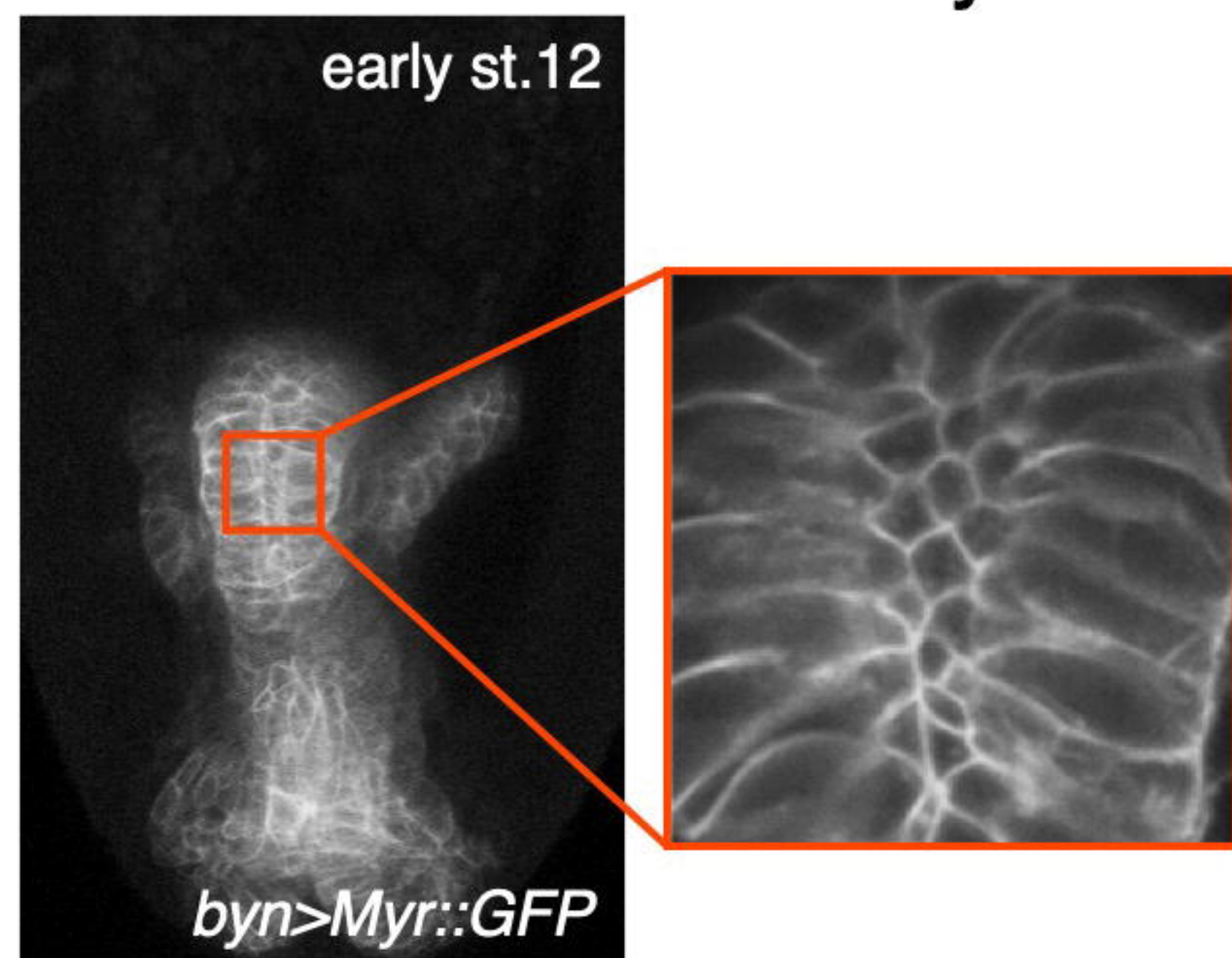
Inverse
Score = 0

(B)

$R^2 = 0.9561$

$p < 0.001$

Mean of Laterality Score

Mean Chirality Index

WT
($N_x = 8, N_y = 114$)

emc^{AP6}
($N_x = 10, N_y = 66$)

$NP2432 > da$
($N_x = 5, N_y = 64$)

$da^{10}; emc^{AP6}$
($N_x = 7, N_y = 114$)

$NP2432 > emc$::GFP in emc^{AP6}
($N_x = 6, N_y = 107$)

$NP2432 > MyoID$::RFP in emc^{AP6}
($N_x = 5, N_y = 51$)

$NP2432 > da > MyoID$::RFP
($N_x = 4, N_y = 83$)

$MyoID^{K2}$
($N_x = 5, N_y = 64$)

$NP2432 > MyoID$::RFP in $MyoID^{K2}$
($N_x = 4, N_y = 98$)

$NP2432 > MyoIC$
($N_x = 6, N_y = 67$)
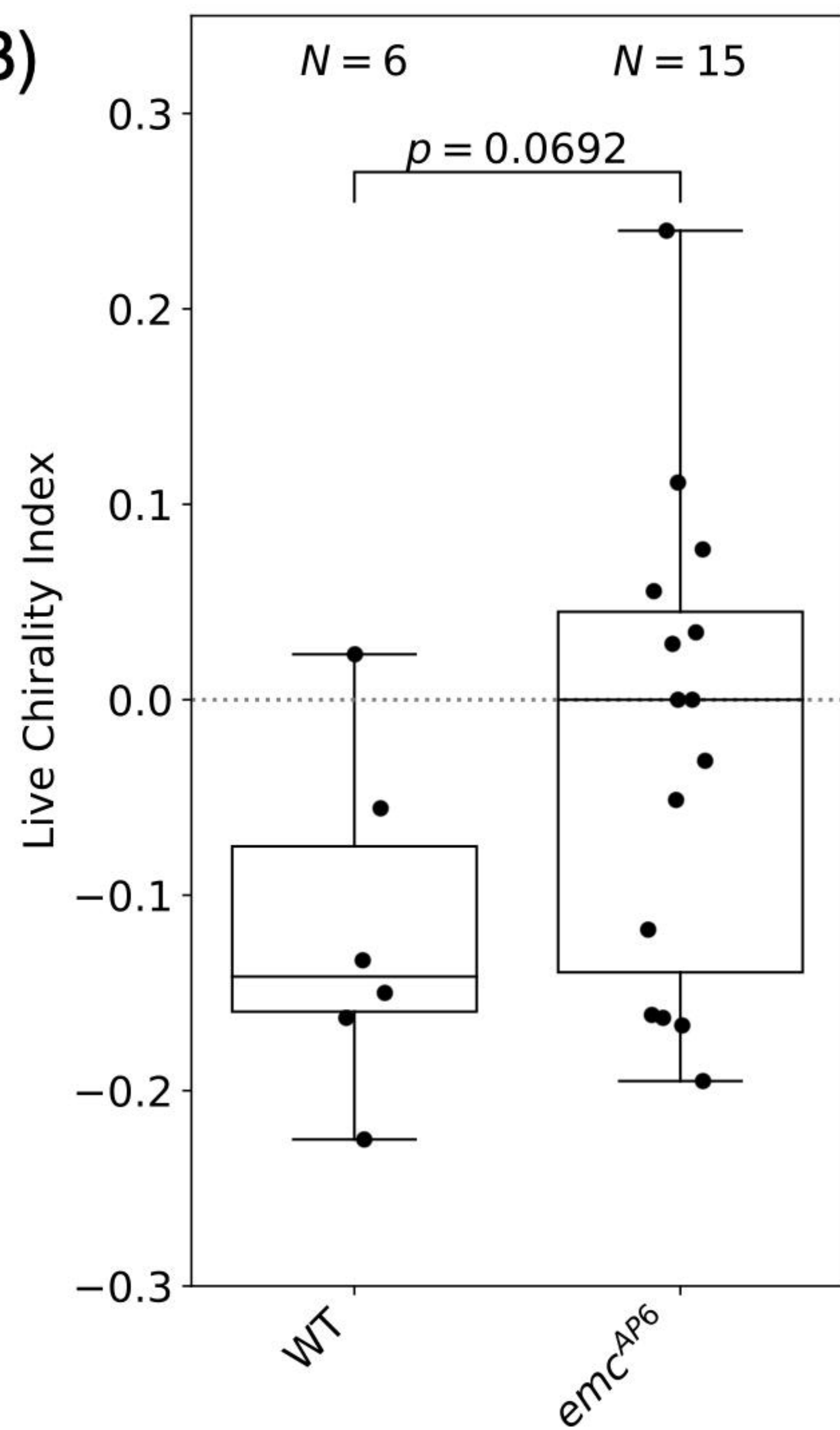
(A) Measure the live chirality index — early st.12 — *byn>Myr::GFP* — Culture for 3 hrs → Evaluate the rotational direction — st.14

(B) $N = 6$ $N = 15$ $p = 0.0692$ — Live Chirality Index — WT — emc^{AP6}

(C) Best fit model $R^2 = 0.8608$ — Model for Figure 2 $R^2 = 0.7247$ — $N = 15$ — Laterality Score — Live Chirality Index